mining

MDPI

Article

The Use of Saudi Silspar as a Ceramic Raw Material

Mohammed Al-Aqydy, Ahmad M. Al-Saleh * and Talal Ghazi Alharbi

Department of Geology and Geophysics, Faculty of Science, King Saud University, P.O. Box 2455, Riyadh 11451, Saudi Arabia
* Correspondence: alsaleh@ksu.edu.sa

Abstract

Feldspar and quartz are essential ceramic raw materials, with feldspar acting as a flux and quartz as a structural filler. Feldspathic sand derived from granitic masses of the eastern Arabian Shield represents a promising local source. This study evaluates upgraded granitic detritus, commercially termed silspar, from the Khurs granite of the Dawadimi terrane. Twenty-five samples were chemically and technologically characterized; one compositionally anomalous sample (S2) was retained in the analytical tables for transparency but excluded before resource-level statistical preprocessing. Pearson correlation, principal component analysis and Ward hierarchical clustering were applied to 24 representative samples using eight chemical variables, while shrinkage, loss on ignition (LOI), whiteness (L*) and water absorption were used for external technological validation. Four chemistry-defined groups were identified: S1 and S3 form a dark impurity-rich pair; S4–S9 form the cleanest ceramic-grade group; S10–S13, S15–S17 and S24 define a transitional Ca-Fe-influenced group; and S14, S18–S23 and S25 form a more coherent potassic group. The firing variables differ significantly among the chemistry-defined groups under the standardized laboratory procedure. The results support controlled ceramic use of the representative Khurs-derived silspar, subject to stockpile homogenization and impurity control. Because phase proportions are normative estimates rather than direct XRD determinations, the work is presented as an integrated preliminary industrial-mineral screening assessment rather than a complete quantitative mineral-phase characterization.

Keywords: Arabian Shield; granite; feldspar; silspar; ceramic

1. Introduction

Feldspar constitutes one of the most important industrial minerals used in ceramic manufacturing due to its dual role as a fluxing agent and a source of alkali oxides and alumina [1,2]. During firing, feldspar promotes liquid-phase formation, enhances densification, and improves both mechanical strength and surface quality of ceramic products [3,4]. For this reason, the performance of ceramic bodies is strongly dependent on feldspar chemistry, particularly alkali content. The rapid expansion of construction and ceramic industries in Saudi Arabia has increased the demand for stable and locally sourced ceramic raw materials. Although feldspathic deposits are widely distributed across central Saudi Arabia, many occurrences contain variable proportions of quartz, clay minerals, and iron-rich accessory phases, which limit their direct industrial application. Consequently, the economic utilization of these resources depends largely on effective beneficiation to achieve compositions compatible with ceramic industry requirements.

Beneficiation of feldspathic raw materials commonly involves integrated processing routes that combine size classification, magnetic separation and froth flotation to concen-

Check for updates

Academic Editor: Juan María Menéndez-Aguado

Received: 29 July 2026
Revised: 2 September 2026
Accepted: 4 September 2026
Published: 10 September 2026

Copyright: © 2026 by the authors. Licensee MDPI, Basel, Switzerland. This article is an open access article distributed under the terms and conditions of the Creative Commons Attribution (CC BY) license.

trate feldspar and reduce deleterious impurities [5]. These techniques have been applied successfully in numerous processing studies and remain standard practice for producing ceramic-grade concentrates from naturally heterogeneous deposits. A common primary source of feldspar is leucocratic granite or pegmatite, which is conventionally extracted, crushed, screened and purified of mafic constituents to yield a product composed mainly of feldspar with variable quartz contents [6]. A more economical alternative is feldspathic sand, consisting mainly of sand-sized detritus derived from erosion of leucocratic granitic masses. Upgrading produces silspar, a purified feldspar–quartz mixture [7,8]; comparable commercial materials include lithospar, minspar and sandspar. Use of such detrital feed can reduce quarrying and crushing requirements, making silspar a practical alternative ceramic raw material [9]. Its quartz component also acts as an essential structural filler that contributes strength and helps control firing shrinkage and mechanical behaviour.

Feldspathic raw materials used by the ceramic and glass industries include potassic, sodic and intermediate feldspars, as well as feldspar–quartz mixtures [10]. Potash feldspar typically melts at approximately 1200 °C, whereas soda feldspar melts at a lower temperature of approximately 1170 °C. Potassic feldspars are commonly used in medium- to high-temperature glazes and ceramic bodies, whereas sodic feldspars are widely used in lower-temperature glass and ceramic-tile formulations [11]. Although specifications and formulation ratios vary by product, the feed delivered from the quarry must remain compositionally consistent.

Within this context, feldspars of the Riyadh region, derived from the erosion of Arabian Shield granitoids, represent a potentially significant yet underutilized industrial mineral resource. Previous exploration efforts were directed specifically towards the assessment of feldspathic sands in various parts of the Arabian Shield, with identified resources of more than 100 million tons of feldspathic wadi sand reported from parts of the NW shield [12]. The present study focuses on the assessment of granitic sand and the upgraded silspar product in the eastern Arabian Shield, integrating geological, mineralogical, and beneficiation testing to evaluate the potential of these materials and their suitability as a domestic source of feldspar for ceramic applications.

2. Local Geology

The eastern Arabian Shield is characterized by granitic batholiths that shed abundant feldspathic sand and gravel across the adjacent desert plains. Favourable sources of relatively clean granitic detritus occur on denuded, slightly elevated surfaces surrounded predominantly by granitic outcrops, where contamination from the volcanosedimentary rocks common elsewhere in the Shield is minimized. The largest batholiths in the eastern Shield occur within the Dawadimi terrane (Figure 1). One of the most important is the Ar Ruwaydah suite, an Ediacaran (611 Ma) A-type post-orogenic intrusive complex [13–15] comprising the Khurs laccolith and the adjoining Arwa ring dyke (Figure 2).

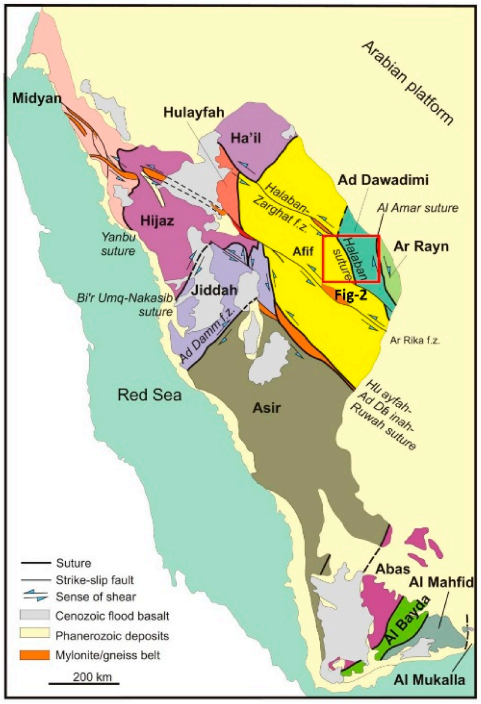


Figure 1. Map of the Arabian Shield showing its constituent terranes and suture (after Johnson [16]).

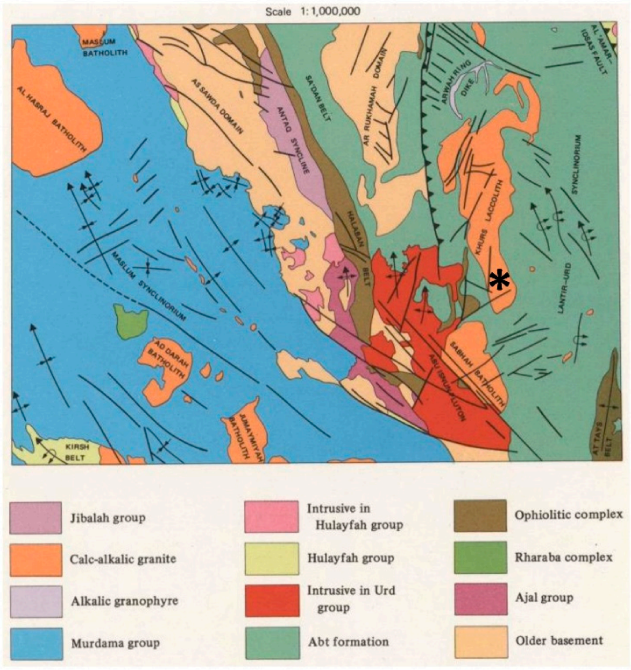


Figure 2. Sketch geologic map of the Dawadimi terrane showing the Khurs pluton; the study area is indicated with an asterisk at the southern tip of the intrusion (after Delfour [17]).

These intrusions cut the Abt schist, a greenschist–facies metamorphic succession interpreted as an accretionary-wedge assemblage formed in the marginal basin of an ensialic island arc [18,19]. The Ar Ruwaydah suite differs from the younger post-tectonic Abanat batholith (584–566 Ma) farther north in being less alkaline and lacking reported rare-metal mineralization [16,20]. Petrographically, the Khurs granites are undeformed, massive, medium-grained, leucocratic and peraluminous monzogranites to syenogranites. They consist principally of quartz (SiO_2), plagioclase, alkali feldspar and biotite, with subordinate hornblende and accessory apatite, titanite and opaque minerals [21]. This

felsic, coarse-grained assemblage makes the Khurs intrusion a favourable source of feldspar–quartz detritus.

The petrographically examined specimens from the Khurs intrusion are pale pink, hypidiomorphic and coarse-grained (Figure 3a), and locally contain large K-feldspar crystals that impart a porphyritic texture. Quartz forms approximately 25–37% of the rock and occurs as clusters of anhedral grains. Orthoclase is the dominant feldspar and commonly displays patch and string perthite (Figure 3b), with local alteration to clay minerals and sericite (Figure 3c). Sodic plagioclase occurs as colourless, subhedral prismatic oligoclase and may form zoned phenocrysts (Figure 3d); antiperthitic intergrowths were not observed. Brown to pale-yellow biotite is commonly the principal mafic mineral and constitutes less than 7% of the examined thin sections. Colourless to weakly pleochroic muscovite occurs locally as interstitial flakes.

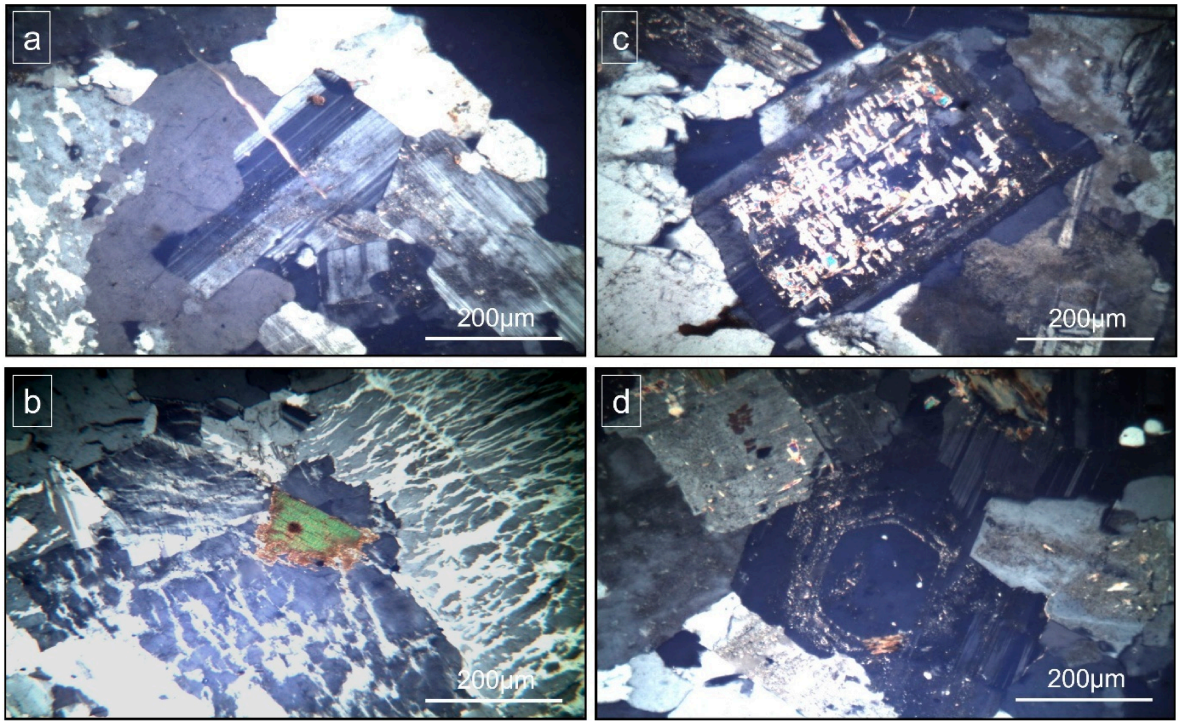


Figure 3. Transmitted-light photomicrographs of the Khurs granite: (**a**) hypidiomorphic granular texture with twinned plagioclase, perthitic K-feldspar and quartz, and only sparse mafic phases (crossed polars, 40×); (**b**) orthoclase showing string perthite (crossed polars, 40×); (**c**) sericitic alteration of plagioclase (crossed polars, 40×); and (**d**) concentric zoning in plagioclase accentuated by micaceous inclusions (crossed polars, 40×).

Figure 3 documents the coarse-grained textures and principal mineral relationships of the parent Khurs granite by transmitted-light petrography; it does not represent the macroscopic appearance, particle-size distribution or sorting of the surficial granitic detritus. Figure 4 provides quarry-scale spatial context, whereas Figure 5 documents the quarry-stage process sequence. Dedicated, scale-calibrated macrophotographs of individual granular samples were not acquired systematically during the original campaign. Accordingly, the stated 3–6 mm product size is the operational screening specification and is not inferred from image-based granulometry. The absence of systematic macrovisual documentation limits independent assessment of grain-size sorting, quarry-face texture and macroscopic heterogeneity. Future sampling campaigns should therefore include standardized close-range photographs of the source material, weathered detritus and beneficiated product, each with a physical scale and an explicit link to the corresponding sample record.

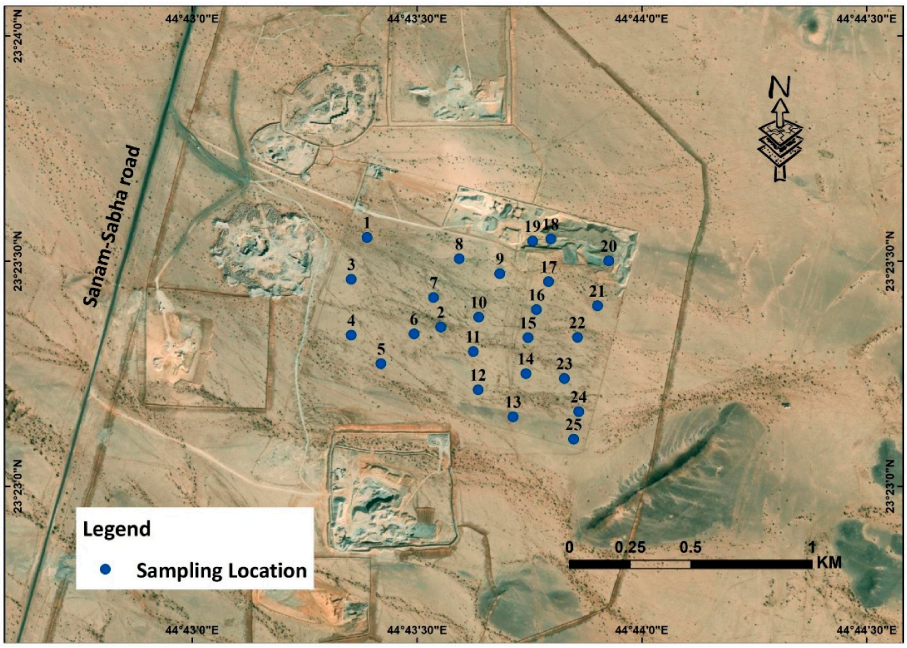


Figure 4. Sample locations within the EXA quarry; the extensive workings in this part of the Khurs pluton are used for extraction of decorative granite.

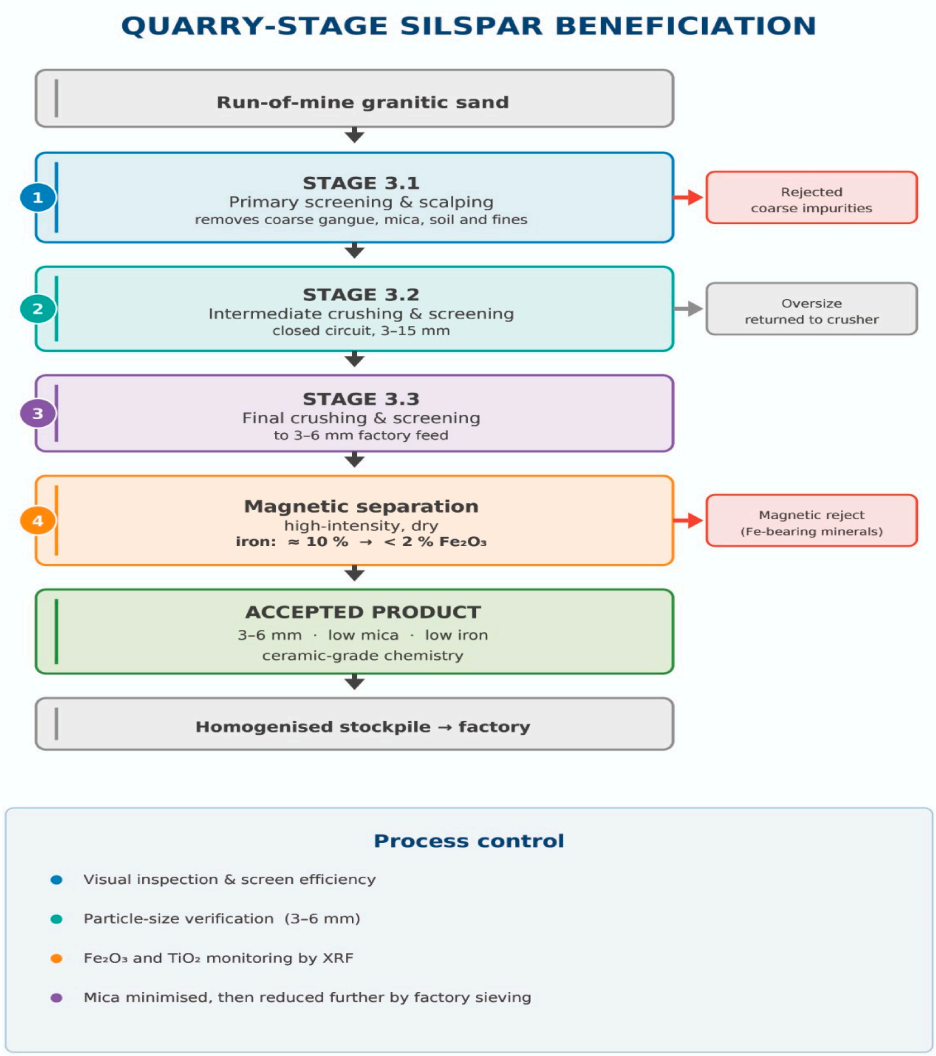


Figure 5. Flow chart showing the sequence of preliminary on-site beneficiation.

3. Quarry-Stage Beneficiation

The study area is located east of the Sanam-Sabha highway, within a quarry licenced to EXA ceramics (Figure 4), a subsidiary of the Al-Fanar Group Ltd (Riyadh, Saudi Arabia). The district on both sides of this road has several mining leases for the quarrying of the Ruwaydah granite, valued for its vivid pink hue and coarse texture. The EXA site is the only operation in the Sanam concession region devoted solely to the extraction of surficial material rich in granitic detritus, and thus represents a pioneering endeavour for the utilization of silspar in the local ceramics industry. Preliminary upgrading is performed on site, with the final processing and beneficiation carried out at the EXA factory in the Second Industrial City in Riyadh.

A total of 25 representative samples were collected across the active working faces of the EXA quarry near the southern margin of the Khurs pluton. Sampling targeted surficial granitic detritus after removal of loose overburden, thereby minimizing contamination by wind-blown sand and surface organic matter. At each station, material was collected from a footprint not exceeding 2 m^2 so that each sample integrated local variability. Each field sample weighed approximately 2 kg and consisted of coarse granitic sand within the operational 3–6 mm product-size interval described in Section 3.3. Each sample was thoroughly mixed and reduced by successive coning and quartering before subsampling for chemical and technological testing. The 25 stations were distributed across the quarry to capture the spatial heterogeneity reflected in the chemical and mineralogical data.

The quality of the final tile body depends strongly on mineral purity, particle-size control, iron-oxide removal and the chemical consistency of incoming raw materials. Feldspar is particularly important because it supplies alumina and alkali fluxes that promote vitrification during firing. In white or light-coloured ceramic bodies, feldspar purity is consequently linked to fired whiteness, dimensional stability, surface quality and final technical performance. Beneficiation is required because granitic sand may contain mica, iron-bearing minerals, clay-rich fines and other gangue phases.

The objective of the quarry-stage operation is to convert run-of-mine silspar into a clean, controlled-size, low-iron ceramic feed suitable for stable factory processing. This stage is not merely a mechanical size-reduction operation; it is a beneficiation sequence designed to remove visible and mineralogical impurities, reduce mica and iron-bearing contaminants, and deliver a particle-size range that can be handled reliably by the plant's milling and dosing systems. In ceramic raw-material processing, the general beneficiation operations include comminution, purification, sizing, classification, and magnetic separation (Figure 5); these operations may be performed at the quarry, at an intermediate treatment facility, or at the manufacturing plant.

3.1. Primary Screening and Impurity Rejection

The first treatment stage consists of primary screening and scalping of the sand extracted from the quarry. This operation removes coarse contaminants, mica flakes, discoloured mineral fragments, soil, clay-rich fines and other visible gangue before the material enters the crushing circuit. The operation is controlled visually and by screen performance rather than by a fixed accept/reject threshold. Visible contaminants are progressively minimized, and residual mica is reduced further during subsequent factory wet sieving. This procedure lowers the load on downstream crushers and separators and avoids excessive comminution of contaminants that would become more difficult to remove at finer sizes.

3.2. Intermediate Crushing and Secondary Screening

After primary screening, the sand is crushed and screened again; the purpose of this second stage is to reduce the particle size while maintaining an intermediate granulometric window, typically 3–15 mm, according to the plant requirements. This particle-size range is large enough to avoid excessive fines generation at the quarry but small enough to allow efficient feeding, conveying, and later final size reduction. This stage is operated as a closed or semi-closed crushing-and-screening circuit. Oversize material is returned to the crusher, while undersize or excessive fines are either removed or blended only if they meet the chemical and mineralogical specifications. In ceramic raw-material preparation, comminution improves impurity liberation, modifies particle-size distribution, facilitates mixing and forming, and produces a more reactive material for firing.

3.3. Final Crushing, Screening, and Magnetic Separation

The third quarry-stage operation is final crushing to the factory feed size of 3–6 mm. This granulometric control is important because the factory dosing and continuous-milling systems require a predictable feed. A stable feed size supports consistent mill loading, grinding efficiency and batch-to-batch reproducibility. After final crushing, the material is screened to remove oversize particles and excessive fines, then passed through high-intensity dry magnetic separators to remove ferromagnetic and paramagnetic contaminants, particularly iron-bearing accessory minerals. Iron in run-of-mine material may approach approximately 10% as Fe_2O_3, whereas the accepted product is controlled to a target of $Fe_2O_3 < 2\%$. The mass yield of the magnetic reject was not recorded during the original campaign; therefore, no quantitative reject percentage is reported. Separation performance is assessed operationally from the iron content of the accepted product, consistent with the Fe_2O_3 values of $\leq$2% in Table 1.

Table 1. Chemical analysis of silspar samples.

Sample	SiO_2	Al_2O_3	K_2O	Na_2O	CaO	Fe_2O_3	SO_3	ZnO	Oxide Total	LOI (%)
S1	63.8	14.9	5.8	4.8	4.6	2.0	0.9	0.4	97.2	1.1
S2	32.7	6.5	2.6	3.1	1.9	1.0	0.5	0.2	76.9	22.6
S3	66.9	13.9	5.9	4.3	4.4	1.5	0.7	0.3	97.8	1.6
S4	74.1	13.7	6.4	3.6	1.0	0.5	0.1	0.0	99.5	0.3
S5	74.2	13.4	6.5	3.7	1.1	0.4	0.1	0.1	99.5	0.4
S6	73.8	13.8	6.6	3.8	1.0	0.4	0.1	0.1	99.5	0.3
S7	74.5	13.7	6.3	3.3	1.1	0.5	0.1	0.1	99.5	0.3
S8	73.6	13.1	5.2	5.0	1.2	0.8	0.1	0.1	99.0	0.6
S9	73.9	13.8	6.4	3.4	1.4	0.5	0.1	0.1	99.6	0.2
S10	68.9	15.4	6.4	0.7	3.1	2.0	0.1	0.1	96.6	1.7
S11	66.3	14.2	8.2	2.2	3.0	1.9	0.1	0.1	95.9	0.9
S12	65.2	15.2	8.5	2.0	2.0	2.0	0.0	0.1	95.1	0.7
S13	66.2	14.3	9.2	3.0	1.5	1.0	0.0	0.0	95.2	0.7
S14	71.1	12.3	8.2	2.0	2.0	1.5	0.0	0.0	97.1	0.8
S15	68.2	13.5	8.0	2.0	0.9	0.3	0.1	0.1	93.0	0.8
S16	66.2	15.0	8.0	3.5	1.3	1.1	0.0	0.1	95.1	0.7
S17	67.3	13.8	8.5	2.9	0.7	2.0	0.0	0.1	95.4	0.5
S18	71.2	12.5	8.2	2.0	1.8	0.8	0.1	0.0	96.6	0.4
S19	69.3	13.2	9.0	2.5	2.0	1.1	0.0	0.0	97.1	0.5
S20	70.1	12.5	8.5	3.0	1.8	1.0	0.0	0.0	97.0	0.4
S21	69.2	13.5	9.2	2.4	2.0	1.0	0.0	0.0	97.4	0.6
S22	71.0	12.0	8.2	2.8	1.7	1.0	0.0	0.0	96.8	0.5
S23	74.2	12.1	8.2	1.9	2.1	0.5	0.1	0.0	99.0	0.4
S24	66.3	15.2	8.1	3.2	2.5	0.9	0.0	0.0	96.2	0.5
S25	72.5	11.5	10.0	2.8	1.8	0.4	0.0	0.0	99.2	0.7

The accepted quarry product should therefore be defined by four criteria: the required 3–6 mm size distribution, low visible mica content, low iron-bearing contaminants, and a chemical specification suitable for the intended ceramic body. For high-quality ceramic applications, the monitoring of Fe_2O_3 and TiO_2 is especially important because these oxides strongly influence fired colour and whiteness. Long-term industrial practice on feldspar beneficiation has shown that magnetic separation can significantly reduce Fe_2O_3 and TiO_2 contents and produce concentrates suitable for ceramics [22,23].

4. Ceramic Tile Manufacturing Process

The factory stage converts the beneficiated raw materials into a pressed, dried, decorated, fired, sorted, and packed ceramic tile. The process sequence described below follows the industrial dry-pressing route used for ceramic tile bodies at the EXA factory: batching, wet milling, slip homogenization, sieving and magnetic purification, spray drying, powder storage, pressing, drying, glazing or decoration where applicable, firing, finishing, automatic sorting, and packaging. ISO 13006 [24] defines ceramic tiles as thin slabs made from feldspar, clays and/or other inorganic raw materials, generally shaped by extrusion or pressing, then dried and fired to develop the required properties.

4.1. Technical Batching and Weighing of Raw Materials

The process begins with the controlled batching of the primary ceramic raw materials, typically clay-bearing materials, quartz/silica-bearing materials, and beneficiated silspar according to a technical body formulation. The materials are dosed using large industrial scales, weigh hoppers, or load-cell-controlled feeding systems. Accurate weighing is fundamental because even small deviations in feldspar, clay, or quartz proportions can change the plasticity, milling behaviour, firing shrinkage, vitrification rate, water absorption, fired colour, and mechanical strength of the final tile. Feldspar dosage must be controlled particularly carefully because it contributes fluxing oxides such as Na_2O and K_2O, which promote liquid-phase formation during firing. Too little feldspar may lead to under-vitrification and high water absorption; too much or poorly balanced feldspar may increase deformation, pyroplasticity, warpage, or excessive glassy phase formation.

4.2. Wet Milling in Continuous Mills

The weighed batch is transferred to continuous wet mills, where water is added to produce a ceramic slip suitable for pumping, screening, magnetic purification and spray drying. In the operational formulation used at the plant, water addition is approximately 59–60% on the plant-defined batch basis; process control is achieved through slip density, viscosity, sieve residue and pumpability rather than through percentage alone. Alumina grinding media are used to minimize contamination from steel. Sodium silicate and soda ash are added at approximately 0.6–0.8% as deflocculants and processing aids to disperse clay-rich particles, reduce slip viscosity and support a high solids content.

4.3. Slip Transfer, Homogenization, Sieving, and Magnetic Purification

After milling, the ceramic body exists as a liquid suspension known as slip; this fluid is transferred to large ground or underground storage tanks equipped with heavy-duty agitators or mixing turbines. The purpose of these tanks is active homogenization, not passive storage. Continuous agitation maintains suspension, minimizes settling, equalizes density and viscosity, and reduces batch-to-batch variation before spray drying. Between the mill, storage tanks, pumps, sieves, and spray dryer feed system, magnetic units should be installed wherever practical to remove residual iron-bearing particles. This is a critical control point because iron contamination may originate not only from the quarry but also from handling equipment, conveyors, mill components, valves, pumps, or maintenance

debris. Magnetic separation can be used for both dry powders and wet slurries to remove magnetic impurities. Before spray drying, the slip must pass through sieving systems to remove coarse particles, agglomerates, unground residues, or foreign matter. Sieving of the wet-ground slip is a recognized method for eliminating contaminants before spray drying.

4.4. Spray Drying: Conversion of Slip into Press Powder

The homogenized and screened slip is pumped to the spray dryer, where it is atomized into fine droplets and contacted with hot air generated by a burner. The inlet air temperature may reach approximately 550 °C, causing rapid water evaporation and formation of free-flowing granules. The spray-dried powder exits with a residual moisture content of approximately 5–6%, suitable for pressing. Moisture and granule-size distribution are critical: insufficient moisture can reduce plasticity and green strength, whereas excess moisture can promote sticking, density gradients and delayed drying.

4.5. Powder Transfer to Silos and Conditioning

The spray-dried powder is transferred to storage silos; the powder should remain in the silos for at least two hours before pressing. This conditioning period allows the powder temperature to decrease, moisture to equilibrate among granules, and the powder bed to stabilize before press feeding. This stage is often underestimated, but it is essential for uniform compaction. Uneven powder temperature or moisture distribution may cause density gradients in the pressed tile, leading to differential shrinkage, warpage, cracking, or dimensional instability during firing. Magnetic units should also be installed between powder storage and the press feed system to capture any remaining metallic or iron-bearing contamination before the body is compacted.

4.6. Dry Pressing of the Ceramic Body

The conditioned powder is then fed to hydraulic presses, where it is compacted inside steel dies to form the green tile. According to international standards, dry-pressed tiles are formed from a finely milled body mixture and shaped in dies or moulds at high pressure. Pressing transforms the spray-dried powder into a coherent green body with defined dimensions, thickness, and density. The key variables are powder moisture, granule flowability, filling uniformity, press pressure, pressing cycle, die condition, and ejection behaviour. The goal is to obtain uniform green density across the tile. Non-uniform density is one of the main causes of firing deformation, size variation, corner lifting, cracks, and post-firing flatness defects.

4.7. Drying of Pressed Tiles

After pressing, the green tiles are dried to remove residual physical moisture before glazing and firing. Drying must be controlled to avoid differential shrinkage, warping, cracking and distortion. Industrial dryers use controlled heated air, with operating temperatures reaching approximately 250 °C, and may recover heat from kiln-cooling zones to improve energy efficiency. The drying profile must be matched to tile thickness, body formulation, green density and powder moisture. Excessively rapid surface drying can create stress gradients, whereas incomplete drying can cause defects during firing.

4.8. Surface Preparation and Glazing

If the product is glazed, the dried body receives surface layers such as engobe, glaze and decoration. Engobe can improve body coverage, surface uniformity and compatibility between the body and glaze. The glaze forms an impermeable vitreous coating that provides colour, gloss or matte appearance, stain resistance and functional surface properties. Glaze formulations may include quartz, feldspar, carbonates, borates, zircon and frits, and

are commonly applied by spraying or other controlled application methods. Before firing, surface moisture, glaze weight, decoration alignment and visible cleanliness are controlled.

4.9. Firing in the Kiln

During firing in the roller kiln, the ceramic body undergoes thermal consolidation, sintering, and vitrification. Firing converts the compacted green body into a dense and mechanically stable ceramic material. The firing parameters that control product quality include peak temperature, soaking time, heating and cooling rate, kiln atmosphere, tile thickness, body composition, and glaze-body compatibility. The kiln temperature may reach approximately 1200 °C, depending on the body type and product specification. At this stage, feldspar plays a central role in promoting liquid-phase formation and densification. Proper firing reduces porosity and improves strength; under-firing may cause high water absorption and weak mechanical properties, while over-firing may cause deformation, bloating, excessive shrinkage, glaze defects, or roller marks. Iron control remains one of the most important quality safeguards throughout the process. Iron oxides and iron-bearing mineral particles can strongly affect fired colour, produce black or brown specks, and induce defect mechanisms under reducing or oxygen-deficient conditions. In ceramic bodies containing carbonaceous matter, Fe_2O_3 may be reduced to FeO, contributing to black-core formation and esthetic or mechanical weakness.

4.10. Cooling, Finishing and Automatic Sorting

After firing, tiles are cooled under controlled conditions to prevent thermal shock, cracking, residual stress, and glaze-body mismatch defects. Depending on product type, additional finishing steps may follow, such as polishing, lapping, squaring, rectification, chamfering, or surface protection. A rectified tile is defined as a ceramic tile that, after firing, is subjected to precise mechanical finishing of the edges. The final stage is automatic sorting; modern sorting lines combine dimensional measurement, visual inspection, shade classification, surface-defect detection, stacking, packaging, and palletizing. Machine-vision systems are used to inspect ceramic tile surfaces, identify defects, classify shade and texture, and reduce the subjectivity of manual inspection. During automatic sorting, tiles are classified by calibre, shade, flatness, edge quality, surface defects, cracks, pinholes, glaze defects, contamination, warpage, and overall grade. Accepted tiles are stacked and packed according to size, shade, calibre, production batch, and quality grade. Rejected or downgraded tiles are separated automatically. This final stage closes the process loop: defects detected at sorting should be traced back to upstream causes such as raw-material contamination, powder moisture, press density, drying behaviour, glaze application, or firing curve instability.

5. Analytical Methods and Results

Major and trace oxide chemistry was determined by energy-dispersive X-ray fluorescence (ED-XRF) using a benchtop EDX-8000 spectrometer (Shimadzu Corporation, Kyoto, Japan) in the EXA quality-control laboratory. The quantified oxides were SiO_2, Al_2O_3, K_2O, Na_2O, CaO, Fe_2O_3, SO_3 and ZnO. Loss on ignition (LOI) was determined gravimetrically after firing. ED-XRF was selected for its efficiency, limited sample-preparation requirements and suitability for routine analysis of powdered silicate raw materials. The chemical results are presented in Table 1.

Excluding S2, the samples are silica-rich and broadly consistent with feldspar–quartz detritus derived from the Khurs granite. SiO_2 ranges from 63.8 to 74.5 wt%, Al_2O_3 from 11.5 to 15.4 wt%, K_2O from 5.2 to 10.0 wt% and Na_2O from 0.7 to 5.0 wt%. Fe_2O_3 does not exceed 2.0 wt% in the beneficiated samples and is compatible with the operational ceramic-feed

criteria used in this study [25], although its variation, together with CaO, SO_3 and ZnO, indicates a variable accessory-mineral contribution and supports controlled blending. S2 is compositionally anomalous (SiO_2 = 32.7 wt%, Al_2O_3 = 6.5 wt% and LOI = 22.56 wt%). The phase responsible for this mass loss cannot be identified from the available bulk data. Residual overburden or soil-derived fines, intense alteration, or incorporation of an altered or non-granitic fragment are possible explanations, but none is treated as a confirmed mineralogical diagnosis. Even under limiting assumptions, assigning all measured CaO to calcite and all SO_3 to gypsum accounts for only about 1.72 wt% theoretical volatile loss, far below the measured LOI. S2 was therefore retained in the analytical tables for transparency but excluded before resource-level statistical preprocessing and interpretation.

To obtain a chemistry-based estimate of the main feldspar–quartz proportions in the treated silspar, the normative recalculation proposed by Al-Nakhebi et al. [7] was applied to the bulk oxide data (Table 2). Excluding S2, K-feldspar is the dominant recalculated component, followed by plagioclase and quartz. These values are normative estimates and should not be interpreted as direct quantitative phase determinations. Optical petrography supports identification of the principal coarse-grained minerals of the parent granite but cannot quantify fine-grained alteration products such as kaolinite or illite, poorly crystalline or amorphous material, cryptocrystalline impurities, or minor secondary phases. XRD and thermogravimetric analysis (TGA) would be required for phase-specific verification. Accordingly, the present work should be regarded as an integrated preliminary screening assessment based on field observations, optical petrography of the parent granite, bulk chemistry and comparative ceramic testing, rather than as a complete quantitative mineral-phase characterization. The chemical variability nevertheless supports stockpile homogenization before factory beneficiation.

Table 2. Normative feldspar–quartz proportions estimated from bulk oxide chemistry.

Sample	K-Feld	Plag	Total Feld	Quartz	LOI (%)
S1	34.2	63.0	97.2	2.8	1.1
S2	NA	NA	NA	NA	22.6
S3	34.9	57.6	92.6	7.4	1.6
S4	37.6	35.8	73.4	26.6	0.3
S5	38.5	36.5	75.0	25.0	0.4
S6	38.8	36.8	75.6	24.4	0.3
S7	37.2	33.3	70.5	29.5	0.3
S8	30.8	48.3	79.1	20.9	0.6
S9	37.6	35.5	73.1	26.9	0.2
S10	37.9	21.3	59.2	40.8	1.7
S11	48.4	33.6	82.0	18.0	0.9
S12	50.2	26.9	77.2	22.8	0.7
S13	54.3	32.7	87.1	12.9	0.7
S14	48.4	27.0	75.4	24.6	0.8
S15	47.3	21.1	68.4	31.6	0.8
S16	47.1	36.0	83.1	16.9	0.7
S17	50.2	28.2	78.4	21.6	0.5
S18	48.4	25.8	74.3	25.7	0.4
S19	53.2	31.2	84.4	15.6	0.5
S20	50.0	34.6	84.6	15.4	0.4
S21	54.4	30.4	84.8	15.2	0.6
S22	48.6	32.2	80.8	19.2	0.5
S23	48.4	26.2	74.6	25.4	0.4
S24	48.0	39.6	87.7	12.3	0.5
S25	59.1	32.9	92.0	8.0	0.7

Note: NA, not applicable; normative phase recalculation was not performed for the anomalous sample S2.

Technological tests were performed in the EXA laboratory for linear firing shrinkage, LOI, fired whiteness (CIE L*) and water absorption; results for all 25 samples are reported in Table 3. CIE L*, on a scale from 0 (black) to 100 (white), was measured using an X-Rite RM200QC imaging spectrocolorimeter (X-Rite, Inc., Grand Rapids, MI, USA) under standardized illumination. Linear firing shrinkage and water absorption were determined using the procedures of SASO GSO ISO 13006:2022 under a common laboratory preparation and firing protocol.

Table 3. Physical and ceramic properties of silspar samples.

Sample	Shrinkage (%)	LOI (%)	Whiteness (L*)	Water Absorption (%)
S1	0.11	1.12	32	0.0000
S2	−0.031	22.56	88	0.2200
S3	0.122	1.56	41	0.0000
S4	0.093	0.29	70	0.0510
S5	0.093	0.38	72	0.0512
S6	0.095	0.29	69.5	0.0495
S7	0.097	0.26	70.1	0.0481
S8	0.062	0.61	69.2	0.0721
S9	0.071	0.2	73.7	0.0698
S10	0.09	1.67	46	0.0000
S11	0.0801	0.85	45	0.0002
S12	0.0751	0.74	55	0.0010
S13	0.0825	0.66	54	0.0001
S14	0.1202	0.77	52	0.0002
S15	0.0821	0.8	71	0.0022
S16	0.1041	0.66	60	0.0007
S17	0.1207	0.48	55	0.0044
S18	0.0874	0.44	66	0.0004
S19	0.1251	0.49	62	0.0003
S20	0.1125	0.44	59	0.0007
S21	0.1084	0.58	62	0.0021
S22	0.1241	0.47	62	0.0025
S23	0.0954	0.44	64	0.0035
S24	0.0988	0.51	59	0.0041
S25	0.1204	0.66	66	0.0101

The representative feldspar–quartz samples show low firing shrinkage and LOI, consistent with their predominantly anhydrous mineralogy [26]. S2 is the clear exception, with slight expansion (−0.031%) and an LOI of 22.56%; because the volatile-bearing phase was not identified, this anomaly is not assigned to a specific mineral or organic component. Fired whiteness, expressed as CIE L* [27], varies widely among the representative samples and is lowest in the impurity-rich samples S1 and S3. The very low measured water-absorption values indicate comparatively advanced densification under the standardized laboratory conditions used in this study [28], but they should not be interpreted as absolute predictors of industrial tile performance. S2 again behaves anomalously, with water absorption of 0.220%. Material exhibiting an S2-type chemical and technological anomaly should be segregated from representative quarry feed and should not be incorporated into production stockpiles before analytical verification. Future investigation should include repeat sampling from the corresponding quarry location, replicate LOI determination, verification of sample identity and preparation history, XRD and thermogravimetric analysis (TGA) to determine the nature and temperature range of volatile release. These results support comparative technological evaluation of the representative samples while reinforcing the need for impurity control and stockpile homogenization.

6. Statistical Interpretation

6.1. Statistical Methods and Treatment of S2

The resource-level statistical dataset comprises 24 representative samples and eight chemical variables (SiO_2, Al_2O_3, K_2O, Na_2O, CaO, Fe_2O_3, SO_3 and ZnO). S2 was excluded before calculation of means, standard deviations and z-scores because its extreme LOI, depleted silica–alumina composition and negative shrinkage are inconsistent with the remaining population. PCA and hierarchical clustering were calculated from the standardized eight-variable chemical matrix. Pearson correlations were calculated across the chemical and technological variables for the 24 representative samples. Hierarchical clustering used Euclidean distance and Ward minimum-variance linkage. Solutions from k = 2 to k = 7 were evaluated using the Silhouette coefficient, Calinski–Harabasz index and Davies–Bouldin index. A secondary 12-variable analysis of the same 24 samples was used only as a sensitivity test. Statistical calculations and visualizations were performed in Python 3.12.14 using NumPy 1.26.4, pandas 2.2.2, SciPy 1.13.1 and scikit-learn 1.5.1. Cluster-validation metrics are reported in Table 4.

Table 4. Chemical cluster-validation metrics after exclusion of S2.

k	Silhouette	Calinski–Harabasz	Davies–Bouldin
2	0.5458	13.7891	0.5183
3	0.3810	15.7468	0.7477
4	0.4228	19.9944	0.8623
5	0.4193	20.3743	0.8966
6	0.4082	19.5459	0.7983
7	0.3892	19.0082	0.6679

6.2. Correlations and Principal Components

Pearson correlations show that the strongest chemical association is SO_3-ZnO (r = +0.897). Fired whiteness decreases with Fe_2O_3 (r = −0.860), CaO (r = −0.844) and LOI (r = −0.772), and increases with SiO_2 (r = +0.759). Additional associations include CaO-LOI (r = +0.754), CaO-SO_3 (r = +0.752), SiO_2-Fe_2O_3 (r = −0.730), SiO_2-water absorption (r = +0.714) and K_2O-water absorption (r = −0.628). These coefficients describe associations rather than direct causation. PC1 explains 47.55% and PC2 26.68% of the standardized chemical variance; together they explain 74.23%. PC3 explains 11.10%, giving 85.33% for the first three components (Table 5). PC1 is dominated by ZnO (+0.938), SO_3 (+0.888), CaO (+0.805), Fe_2O_3 (+0.642), Al_2O_3 (+0.630), SiO_2 (−0.626) and K_2O (−0.533). PC2 is controlled mainly by Na_2O (+0.729), K_2O (−0.710), SiO_2 (+0.699) and Fe_2O_3 (−0.637). The integrated sensitivity model explains 70.38% in PC1-PC2 and strongly agrees with the chemical model at k = 4 (adjusted Rand index = 0.860). The PCA score distribution is shown in Figure 6, and the mean standardized chemical profiles are compared in Figure 7.

Table 5. Chemical PCA eigenvalues and explained variance after exclusion of S2.

Component (Eigenvalue)	Explained Variance (%)	Cumulative (%)
PC1 (3.969)	47.55	47.55
PC2 (2.227)	26.68	74.23
PC3 (0.927)	11.10	85.33
PC4 (0.597)	7.15	92.48
PC5 (0.330)	3.95	96.43

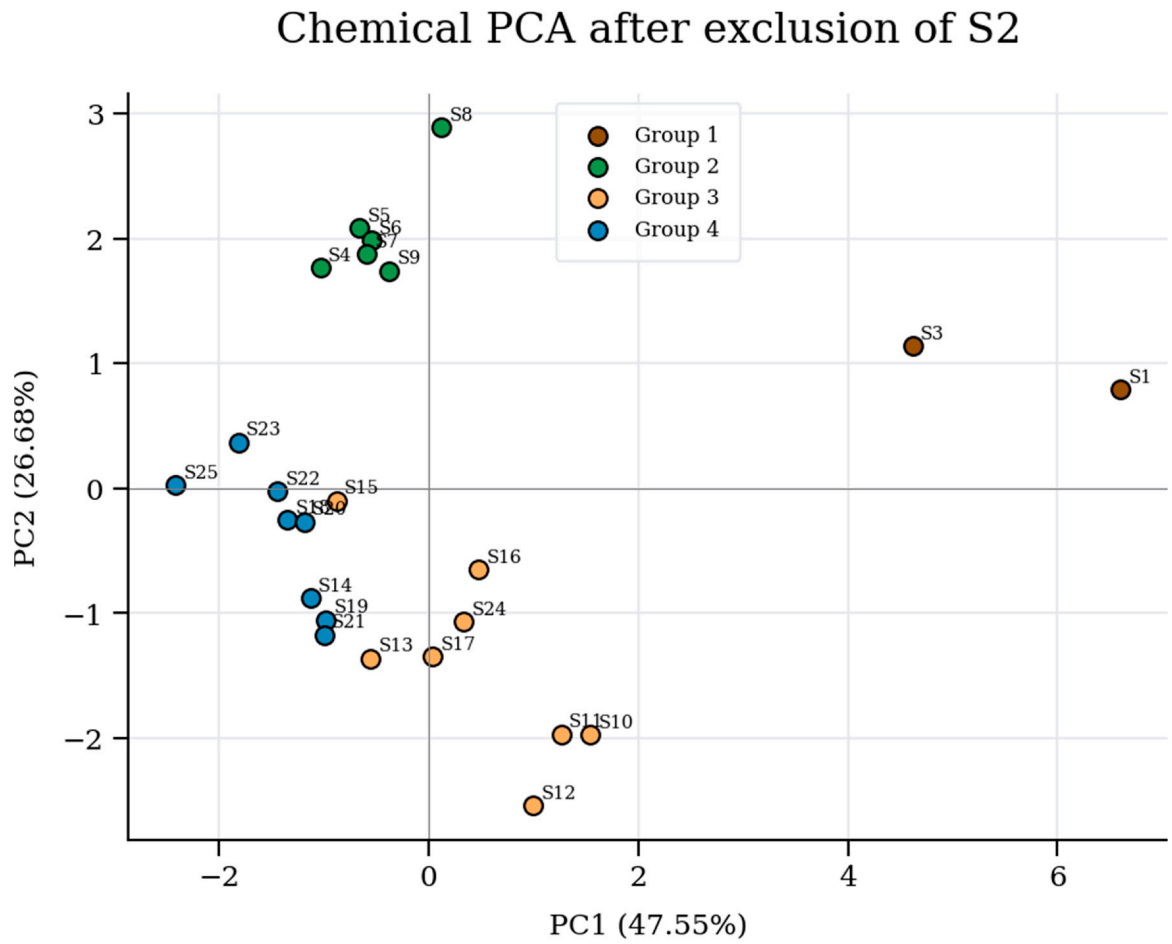


Figure 6. Chemical PCA score plot after exclusion of S2; colours indicate the detailed four-cluster solution.

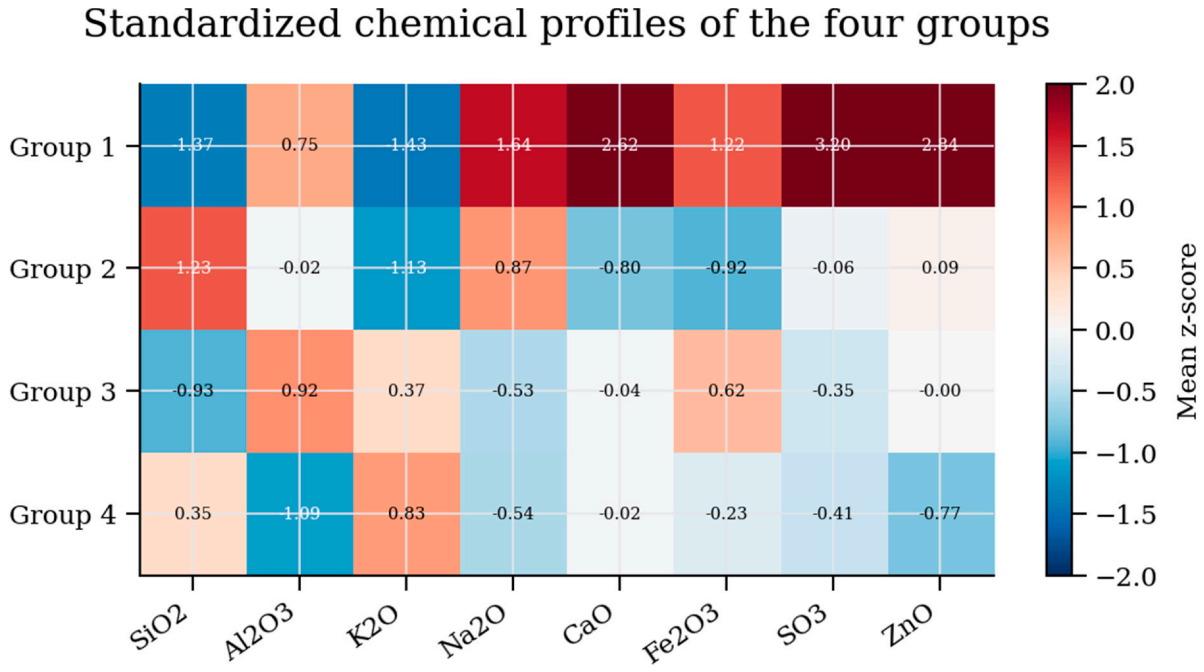


Figure 7. Mean standardized chemical profiles of the four chemistry-defined groups.

6.3. Hierarchical Clustering and Group Selection

The global Silhouette optimum occurs at k = 2 (0.5458), but this solution provides only a coarse separation of the persistent dark, impurity-rich pair S1 and S3 from the other 22 samples. The four-cluster solution provides the most technologically interpretable detailed partition, with Silhouette = 0.4228, Calinski–Harabasz = 19.9944 and Davies–Bouldin = 0.8623 (Table 4). Group 1 comprises S1 and S3; Group 2 comprises S4–S9; Group 3 comprises S10–S13, S15–S17 and S24; and Group 4 comprises S14, S18–S23 and S25. These are chemistry-defined groups, not direct mineral-phase classes. The hierarchical structure is shown in Figure 8. The closest standardized chemical relationships are listed in Table 6, and the final group memberships are summarized in Table 7.

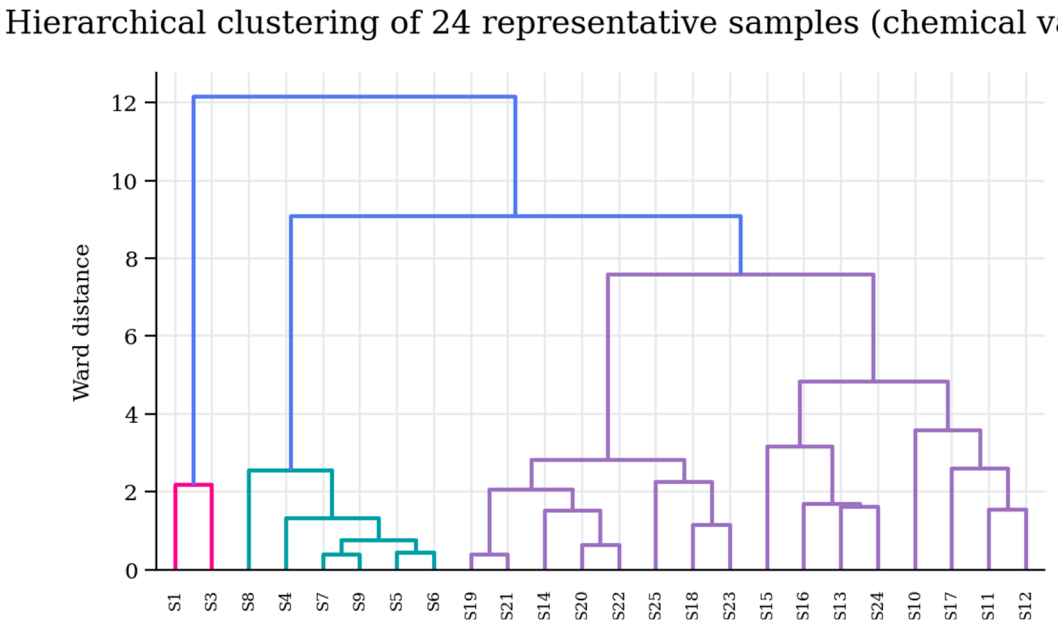


Figure 8. Hierarchical cluster dendrogram for 24 representative samples using eight standardized chemical variables, Euclidean distance and Ward linkage.

Table 6. Top 20 closest relationships based on standardized chemical Euclidean distance.

Sample A	Sample B	Standardized Distance
S19	S21	0.3840
S7	S9	0.3888
S5	S6	0.4296
S5	S7	0.5595
S5	S9	0.6126
S6	S9	0.6248
S20	S22	0.6374
S6	S7	0.6442
S19	S20	0.9949
S4	S6	1.0870
S4	S7	1.0922
S4	S5	1.0979
S18	S22	1.1182
S4	S9	1.1341
S18	S23	1.1548
S18	S20	1.2491
S14	S22	1.2669
S20	S21	1.3035
S14	S18	1.3327
S18	S19	1.4021

Table 7. Four chemistry-defined groups after exclusion of S2.

Group	Samples	Technological Interpretation
1	S1, S3	Dark/impurity-rich pair; cautious use in colour-sensitive bodies.
2	S4–S9	Cleanest high-silica ceramic-grade group.
3	S10–S13, S15–S17, S24	Transitional Ca-Fe-influenced group; controlled blending or beneficiation recommended.
4	S14, S18–S23, S25	More coherent potassic group with promising ceramic potential.

6.4. Independent Technological Validation

Shrinkage, LOI, whiteness and water absorption were not used to construct the primary chemical groups and were therefore evaluated as external technological variables. Because group sizes are unequal and Group 1 contains only two samples, ANOVA results were interpreted together with the non-parametric Kruskal–Wallis test. Significant differences were obtained for shrinkage (ANOVA F = 5.525, $p = 0.0063$; Kruskal–Wallis H = 10.010, $p = 0.0185$), LOI (F = 9.290, $p = 0.00047$; H = 14.836, $p = 0.0020$), whiteness (F = 19.456, $p = 3.80 \times 10^{-6}$; H = 15.402, $p = 0.0015$) and water absorption (F = 131.171, $p = 2.53 \times 10^{-13}$; H = 15.683, $p = 0.0013$). Concordance between the parametric and rank-based tests supports a technological distinction among the chemistry-defined groups, although inference for Group 1 remains cautious.

6.5. Chemical Controls on Ceramic Firing Behaviour

Under the common preparation and firing conditions, differences in shrinkage, water absorption and fired whiteness can be interpreted in relation to bulk composition. K_2O and Na_2O supplied by feldspar act as fluxing oxides and promote liquid-phase formation, densification and progressive pore closure. The silica–alumina–alkali balance governs both the quantity and viscosity of the liquid phase. Fe_2O_3 is associated with lower fired whiteness and may contribute to colour development or dark defects, whereas elevated CaO together with Fe_2O_3 may indicate a greater contribution from Ca-rich plagioclase and/or mafic accessory material. These tests are controlled comparative measures, not absolute predictors of industrial tile performance, which also depends on body formulation, milling, compaction and firing schedule.

7. Conclusions

Feldspar- and quartz-rich granitic detritus derived from the Khurs intrusion represents a chemically promising local ceramic raw material under the investigated test conditions and contains spatially variable minor impurities that require controlled management. Quarry-stage screening, controlled crushing and magnetic separation remain essential for particle-size consistency and impurity reduction, while stockpile homogenization is required to manage compositional variability.

After exclusion of the non-representative S2 sample before statistical preprocessing, the remaining 24 samples define four chemistry-based groups with significantly different comparative firing responses. S4–S9 form the cleanest ceramic-grade group; S10–S13, S15–S17 and S24 form a transitional Ca-Fe-influenced group; S14, S18–S23 and S25 define a more coherent potassic group; and S1 and S3 form a dark impurity-rich pair requiring cautious use in colour-sensitive bodies. S2 remains in the analytical tables for transparency but is not interpreted as part of the representative resource population; its anomalous LOI cannot be assigned to a specific phase from the available data. Material displaying a comparable anomaly should be isolated from production stockpiles pending repeat sampling, replicate LOI measurement, verification of sample identity, XRD and thermogravimetric analysis (TGA). The feldspar–quartz proportions are normative chemistry-based estimates

rather than direct quantitative mineral determinations. The study therefore supports controlled industrial use of the representative material as a preliminary screening assessment while emphasizing selective blending, iron and mica control, standardized macrovisual documentation in future campaigns, and the need for direct phase-specific verification of anomalous or mineralogically uncertain material.

Author Contributions: Conceptualization, M.A.-A., A.M.A.-S. and T.G.A.; Methodology, M.A.-A., A.M.A.-S. and T.G.A.; Software, M.A.-A. and A.M.A.-S.; Validation, M.A.-A., A.M.A.-S. and T.G.A.; Formal analysis, M.A.-A., A.M.A.-S. and T.G.A.; Investigation, M.A.-A., A.M.A.-S. and T.G.A.; Resources, M.A.-A., A.M.A.-S. and T.G.A.; Data curation, M.A.-A., A.M.A.-S. and T.G.A.; Writing—original draft, M.A.-A., A.M.A.-S. and T.G.A.; Writing—review & editing, M.A.-A., A.M.A.-S. and T.G.A.; Visualization, M.A.-A. and A.M.A.-S.; Supervision, A.M.A.-S. and T.G.A.; Project administration, M.A.-A., A.M.A.-S. and T.G.A.; Funding acquisition, M.A.-A. All authors have read and agreed to the published version of the manuscript.

Funding: This research received no external funding.

Data Availability Statement: The original contributions presented in this study are included in the article. Further inquiries can be directed to the corresponding author.

Acknowledgments: This work forms part of the Ph.D. thesis of the first author at the Department of Geology and Geophysics, King Saud University, Riyadh. The authors thank the Deanship of Graduate Studies at King Saud University for its continued support; Abdulaziz Al-Khathlan of the Mining and Hydrocarbon Institute at KACST for technical assistance; and Alfanar Group–EXA Ceramics Company for access to the quarry and analytical support from its R&D laboratories. The staff of the Faculty of Science Research Center are also thanked for their technical support.

Conflicts of Interest: The authors declare no conflict of interest.

References

1. Zhang, Y.; Hu, Y.; Sun, N.; Liu, R.; Wang, Z.; Wang, L.; Sun, W. Systematic review of feldspar beneficiation and its comprehensive application. *Miner. Eng.* **2018**, *128*, 141–152. [CrossRef]
2. Candeias, C.; Gomes, A.; Rocha, F. Assessment of feldspars from Central Portugal pegmatites for sustainable ceramic applications. *Minerals* **2025**, *15*, 527. [CrossRef]
3. Gaied, M.E.; Gallala, W. Beneficiation of feldspar ore for application in the ceramic industry: Influence of composition on the physical characteristics. *Arab. J. Chem.* **2015**, *8*, 186–190. [CrossRef]
4. Winarno, T.; Marin, J.; Ayuningtyas, P.; Herdatama, S.R.; Pudyanarendra, S. The analysis of feldspar characteristics as ceramic material at Mount Ragas, Jepara, Central Java. *IOP Conf. Ser. Earth Environ. Sci.* **2024**, *1339*, 012001. [CrossRef]
5. Huang, H.; Li, S.; Gou, H.; Zhang, N.; Liu, L. Efficient recovery of feldspar, quartz, and kaolin from weathered granite. *Minerals* **2024**, *14*, 300. [CrossRef]
6. Dondi, M.; Conte, S.; Molinari, C.; Zanelli, C. Mineral resources for the ceramic industry: Survey of feldspathic raw materials in Italy. *Minerals* **2025**, *15*, 87. [CrossRef]
7. Al-Nakhebi, Z.; Al-Ghamdi, S.A.; Al-Marzouki, H.; Habib, M.K. *Investigation for Feldspathic Sand and Weathered Leucocratic Granite Deposits Suitable for Feldspar and Silspar Production in the Governorates of Ar Riyad, Al-Madinah al Munawwarah, and Makkah al Mukarramah, Kingdom of Saudi Arabia*; Saudi Geological Survey Open-File Report SGS-OF-2001-6; Saudi Geological Survey: Jeddah, Saudi Arabia, 2001.
8. Ghandourah, A.K.H.; Al Ghamdi, R.A.; Kurdi, S.A.; Zahrani, H.H.; Tamimi, A.H.; Eskander, M.A. *Exploration for Weathered Granite in the Al-Madinah–Yanbu Area as a Source of Silspar*; Saudi Geological Survey Technical Report SGS-TR-Z012-S; Saudi Geological Survey: Jeddah, Saudi Arabia, 2014.
9. Škvarka, J.; Janáková, I.; Pticen, F. Utilising feldspathic overburden and basement rocks from the Vidnava kaolin deposit as secondary raw materials for the ceramic industry. *Physicochem. Probl. Miner. Process.* **2026**, *62*, 226663. [CrossRef]
10. Kogel, J.E. (Ed.) *Industrial Minerals & Rocks: Commodities, Markets, and Uses*; SME: Littleton, CO, USA, 2006.
11. Carter, C.B.; Norton, M.G. *Ceramic Materials: Science and Engineering*; Springer: New York, NY, USA, 2007.
12. Hains, D.; Dickson, T.; Carter, D.; Cullen, M.; Boyd, W. Minerals Inventory and Potential Assessment Report: Kingdom of Saudi Arabia. In *Industrial Minerals*; Saudi Geological Survey: Jeddah, Saudi Arabia, 2016; Volume 2.

13. Robinson, F.A.; Foden, J.D.; Collins, A.S. Zircon geochemical and geochronological constraints on contaminated and enriched mantle sources beneath the Arabian Shield, Saudi Arabia. *J. Geol.* **2015**, *123*, 463–489. [CrossRef] [PubMed]
14. Johnson, P.R. The Arabian–Nubian Shield, an introduction: Historic overview, concepts, interpretations, and future issues. In *The Geology of the Arabian–Nubian Shield*; Springer: Cham, Switzerland, 2021; pp. 1–38.
15. El-Qassas, R.A.; Eldosouky, A.M.; Abd El-Wahed, M.A.; Attia, M.; Ai, H.; Al-Saleh, A.M.; Alarifi, S.S. Unraveling the structural controls and tectonic history of the eastern Saudi Arabian Shield using remote sensing, geological and aeromagnetic data. *J. Asian Earth Sci.* **2026**, *311*, 107225. [CrossRef]
16. Johnson, P.R. *Explanatory Notes to the Map of Proterozoic Geology of Western Saudi Arabia*; Saudi Geological Survey Technical Report SGS-TR-2006-4; Saudi Geological Survey: Jeddah, Saudi Arabia, 2006.
17. Delfour, J. *Geologic Map of the Halaban Quadrangle, Sheet 23G, Kingdom of Saudi Arabia, Scale 1:250,000*; Geoscience Map GM-46C; Deputy Ministry for Mineral Resources: Jeddah, Saudi Arabia, 1979.
18. Cox, G.M.; Lewis, C.J.; Collins, A.S.; Halverson, G.P.; Jourdan, F.; Foden, J.; Nettle, D.; Kattan, F. Ediacaran terrane accretion within the Arabian–Nubian Shield. *Gondwana Res.* **2012**, *21*, 341–352. [CrossRef]
19. Al-Husseini, M.I. The Ediacaran Central Arabia Tectonic Belt (CATEB) in the Arabian Shield. *Middle East Geol. Time Scale* **2024**, *2024*, 1.
20. Robinson, F.A.; Bonin, B.; Pease, V.; Anderson, J.L. A discussion on the tectonic implications of Ediacaran late- to post-orogenic A-type granite in the northeastern Arabian Shield, Saudi Arabia. *Tectonics* **2017**, *36*, 582–600. [CrossRef]
21. Hassan, M.M.; Dessouky, O.K.; Al Shammari, A.M.; Al Barakati, A.N.; Memish, A.N. Petrogenesis and geochemistry of the successive granitic events in the eastern Arabian Shield: Implications for tectonic evolution and crustal thickening. *Int. J. Earth Sci.* **2023**, *112*, 2145–2160. [CrossRef]
22. Wang, H.; Zhao, Y.; Lin, Z.; Shen, L. Efficient separation of iron and alumina in red mud using reduction roasting and magnetic separation. *Min. Metall. Explor.* **2024**, *41*, 1543–1552. [CrossRef]
23. Ku, J.; Wang, K.; Wang, Q.; Lei, Z. Application of magnetic separation technology in resource utilization and environmental treatment. *Separations* **2024**, *11*, 130. [CrossRef]
24. *ISO 13006:2018*; Ceramic Tiles—Definitions, Classification, Characteristics and Marking. International Organization for Standardization: Geneva, Switzerland, 2018.
25. Sinton, C.W. *Raw Materials for Glass and Ceramics: Sources, Processes, and Quality Control*; Wiley: Hoboken, NJ, USA, 2006.
26. Dondi, M.; Raimondo, M.; Zanelli, C. Clays and bodies for ceramic tiles: Reappraisal and technological classification. *Appl. Clay Sci.* **2014**, *96*, 91–109. [CrossRef]
27. Doherty, J. *Porcelain*; A & C Black: London, UK, 2002.
28. Reed, J.S. *Principles of Ceramics Processing*, 2nd ed.; Wiley: New York, NY, USA, 2008.

Disclaimer/Publisher's Note: The statements, opinions and data contained in all publications are solely those of the individual author(s) and contributor(s) and not of MDPI and/or the editor(s). MDPI and/or the editor(s) disclaim responsibility for any injury to people or property resulting from any ideas, methods, instructions or products referred to in the content.